Rodriguez-Garcia, Pedro, Jack Sifri, Caleb Calabrese, Charles Baylis, and Robert J. Marks II.
"Range Improvement in Single-Beam Phased Array Radars by Amplifier Impedance Tuning."
2021 IEEE Texas Symposium on Wireless and Microwave Circuits and Systems (WMCS), Waco, TX

2021 IEEE Texas Symposium on Wireless and Microwave Circuits and Systems (WMCS) | 978-1-6654-0309-2/21/$31.00 ©2021 IEEE | DOI: 10.1109/WMCS52222.2021.9493282

Range Improvement in Single-Beam Phased Array Radars by Amplifier Impedance Tuning

Pedro Rodriguez-Garcia[1], Jack Sifri[2], Caleb Calabrese[3], Charles Baylis[3], and Robert J. Marks II[3]

[1]Raytheon, Dallas, TX, USA
[2]Keysight Technologies, Santa Rosa, CA, USA
[3]Baylor University, Waco, TX, USA

***Abstract*—Significant radar range degradation can be incurred due to variations in antenna impedance from changing array scan angle. Element-wise reconfigurable impedance tuners can be used to optimally match the power amplifier device; however, the impedance matching can also affect the array pattern. In this paper, the effects of element-wise impedance tuning on the transmitted power and on the array pattern are studied, and an approach is recommended for the element-wise implementation of impedance tuners. Examples of impact on array pattern and transmitted power are given using simulation of a designed switched-stub impedance tuner. As a result of these experiments, guidelines are developed for the creation of real-time circuit optimization techniques in the array elements.**

***Index Terms*— cognitive radar, power amplifiers, radar phased array beamforming, radio spectrum management, reconfigurable circuits**

I. Introduction

Transmissions of signals from phased arrays can often suffer from mismatched amplifiers due to mutual coupling, as described by Haupt [12]. To complicate the situation, the mutual coupling changes as the scan angle is adjusted [1]. Reconfigurable circuitry can be used in each of the elements to provide adaptive matching to the power amplifier devices for improvement of output power, power-added efficiency, and/or spectral performance [2]. The advent of high-power reconfigurable matching circuits, as demonstrated by Semnani [4], has opened the possibility of using reconfigurable impedance tuners in radar transmitter elements. Success of impedance tuning in an array environment is expected to be similar to demonstrated benefits of impedance tuning in single-antenna systems to compensate for environmental effects causing antenna impedance changes [5-7]. Impedance tuning is expected to provide benefits beyond wideband matching [8-11], as the optimal match can be individually obtained for each scan angle.

We address the array impedance variation issue by implementing individual tuning of the driven element impedances in a phased array transmitter according to the Fig. 1 diagram as the scan angle changes. Through a co-simulation setup between Keysight Technologies Advanced Design System (ADS) circuit simulation software and ADS Momentum electromagnetic simulation software, we analyze the effect of element-wise reconfigurable circuitry on the range performance of radar, as well on the transmitting array pattern. The results of this work are also expected to be applicable to fifth-generation (5G) wireless communication systems utilizing phased arrays.

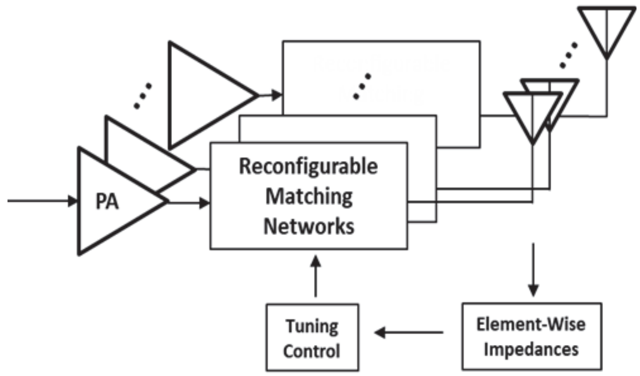

Fig. 1. Block diagram of element-wise array matching circuit configuration

II. Phased Array Impedance Tuning

To enable the ADS/Momentum simulations, a schematic was first generated with a uniform linear array (ULA) of four $\lambda/2$-spaced microstrip patch antenna elements (Fig. 2). The elements were designed using Rogers RO4003C substrate at the design frequency of 3.55 GHz, a frequency presently allocated for sharing between radar and wireless communications in the United States. Nonlinear models for the MWT-173 Gallium Arsenide (GaAs) metal-semiconductor field-effect transistor (MESFET) biased at V_{DS} = 4.5 V and V_{GS} = -1.5 V were connected to the antenna elements.

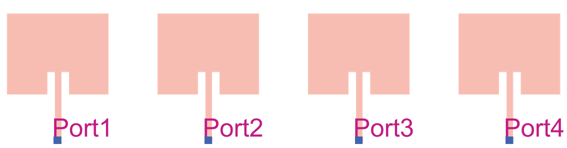

Fig. 2. 4-element $\lambda/2$ uniform linear microstrip array in ADS.

Fig. 3 shows a parameter sweep of the driven element impedances at 3.55 GHz as the array scans from θ_s = -60° to +60° in the $\phi = 0°$ cut that was conducted to observe the mismatch effects of varying the scan angle. In Fig. 3, the driven end element impedances (elements 1 and 4) behave similarly and the driven inner element impedances (elements 2 and 3) behave similarly because of array symmetry.

The four-element array, with the input to each antenna used as a port, can be characterized using the four-port Z-parameters. These parameters give the relationship between the total antenna voltages and currents as follows:

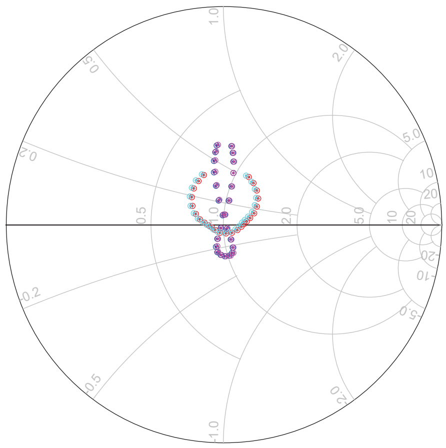

Fig. 3. Parameter swept driven element impedances for scan angles of $\theta_s = -60°$ to $+60°$ at 3.55 GHz for $k_0 = 2\pi/\lambda,\ d = \lambda/2$, end elements (light blue and red), and inner elements (dark blue and purple).

$$\begin{bmatrix} V_1 \\ V_2 \\ V_3 \\ V_4 \end{bmatrix} = \begin{bmatrix} Z_{11} & Z_{12} & Z_{13} & Z_{14} \\ Z_{21} & Z_{22} & Z_{23} & Z_{24} \\ Z_{31} & Z_{32} & Z_{33} & Z_{34} \\ Z_{41} & Z_{42} & Z_{43} & Z_{44} \end{bmatrix} \begin{bmatrix} I_1 \\ I_2 \\ I_3 \\ I_4 \end{bmatrix} \tag{1}$$

The driven element impedances are the apparent impedances seen looking into each antenna, as they are the ratios of voltage to current at the antenna inputs:

$$\begin{aligned} Z_{d1} &= \frac{V_1}{I_1} = Z_{11} + Z_{12}\frac{I_2}{I_1} + Z_{13}\frac{I_3}{I_1} + Z_{14}\frac{I_4}{I_1} \\ Z_{d2} &= \frac{V_2}{I_2} = Z_{21}\frac{I_1}{I_2} + Z_{22} + Z_{23}\frac{I_3}{I_2} + Z_{24}\frac{I_4}{I_2} \\ Z_{d3} &= \frac{V_3}{I_3} = Z_{31}\frac{I_1}{I_3} + Z_{32}\frac{I_2}{I_3} + Z_{33} + Z_{34}\frac{I_4}{I_3} \\ Z_{d4} &= \frac{V_4}{I_4} = Z_{41}\frac{I_1}{I_4} + Z_{42}\frac{I_2}{I_4} + Z_{43}\frac{I_3}{I_4} + Z_{44}. \end{aligned} \tag{2}$$

To steer the beam to a direction θ_s, the individual current sources in (2), for a uniformly spaced linear array, follow the linear phase progression

$$\begin{aligned} I_1 &= |I_1| & I_2 &= |I_2|e^{-jk_0 d\sin\theta_s}, \\ I_3 &= |I_3|e^{-j2k_0 d\sin\theta_s} & I_4 &= |I_4|e^{-j3k_0 d\sin\theta_s}. \end{aligned} \tag{3}$$

where k_0 is the propagation constant of the transmission medium. It is imperative that this phase progression remain unharmed when tuning the driven element impedances in (2) to preserve the integrity of the array pattern. From (3), the first element is typically excited with no phase shift. The next consecutive elements all experience varying phase shifts, so these relative phase shifts should be maintained to provide an undistorted array pattern and steer the array properly to the desired scan angle.

A. Tuning at Broadside

Upon observing these effects, the array was then steered to the broadside ($\theta_s = 0°$) scan angle with identical magnitude and phase current source excitations of each array element. A power-delivered load-pull was then conducted to observe the optimum terminating load impedance that should presented to the amplifier for maximum power delivery. The driven impedances were placed on the same load-pull plot in Fig. 4 to show the power delivered load impedance level in which the un-tuned driven element impedances were located as well as the array pattern. Due to the equality of all four excitation currents, the initial driven element impedances for the broadside case are represented as a special case of equation (2):

$$\begin{aligned} Z_{d1} &= \frac{V_1}{I_1} = Z_{11} + Z_{12} + Z_{13} + Z_{14} \\ Z_{d2} &= \frac{V_2}{I_2} = Z_{21} + Z_{22} + Z_{23} + Z_{24} \\ Z_{d3} &= \frac{V_3}{I_3} = Z_{31} + Z_{32} + Z_{33} + Z_{34} \\ Z_{d4} &= \frac{V_4}{I_4} = Z_{41} + Z_{42} + Z_{43} + Z_{44}. \end{aligned} \tag{9}$$

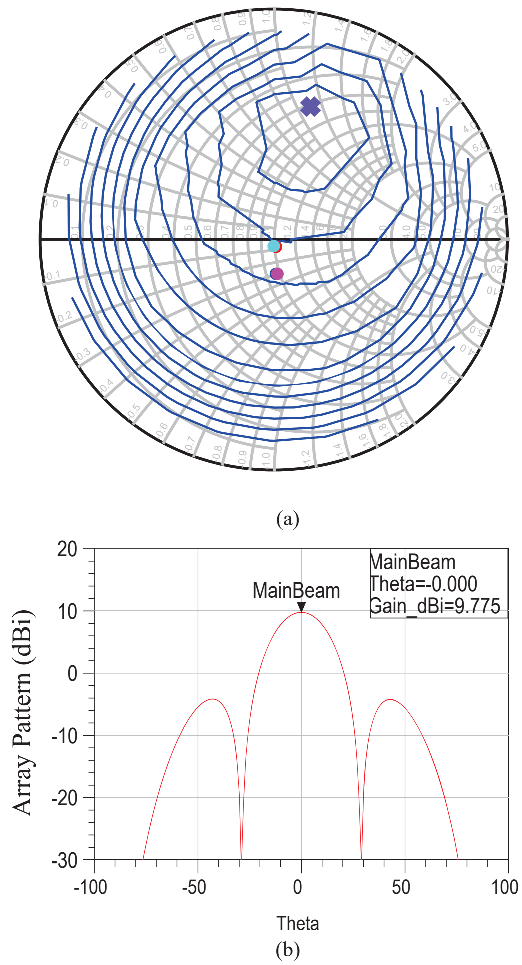

Fig. 4. (a) Untuned driven element impedances for $\theta_s = 0°$, (b) untuned array pattern (dBi).

Fig. 4(a) shows the un-tuned driven element impedances with the output power load-pull contours. The untuned driven element impedances are not located at the maximum output power load impedance, resulting in a significant output power and range reduction.

To mitigate this reduction of radar range and maximize the transmitter output power, the driven element impedances are tuned with models for the switched-state radial stub reconfigurable impedance tuners presented by Calabrese [13]. A tuner is placed between each antenna element and its associated power amplifier. The layout of the tuner and its 3.55 GHz driven element impedance coverage at broadside for each element is presented in Fig. 5.

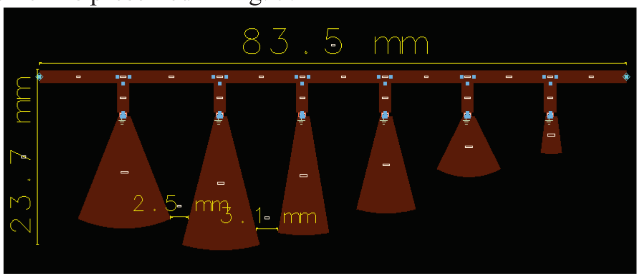

(a)

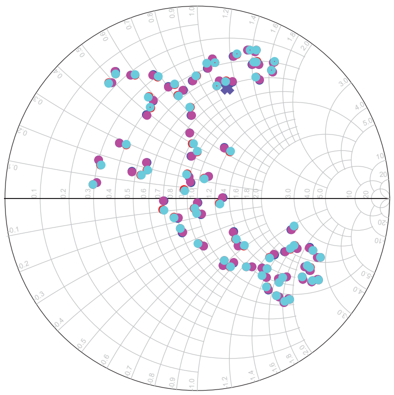

(b)

Fig. 5. (a) Board layout of the switched-state radial stub impedance tuner, (b) tuner element-wise driven impedance coverage for $\theta_s = 0°$ showing closest points to maximum PA power delivered load impedance (purple x-mark) at switch state 111110 for all tuners.

The tuner switch state combination can be represented with a binary sequence. A bit of “1” indicates a radial stub has been activated (presented to the series line by closing the switch), and a bit of “0” indicates a radial stub has not been activated. Since there are a total of six radial stubs in the design, this switched-stub configuration provides a total combination of $2^6 = 64$ unique tuning states. The 3.55 GHz impedance coverage (is sufficient to tune the driven impedances from Fig. 5(a) for the $\theta_s = 0°$ to the optimum power delivered load impedance to be presented to each power amplifier using this reconfigurable impedance tuner design [13]. Tuner losses at the varying switch states, however, may differ significantly since different stubs are “activated” and “deactivated” according to the switch state. This means that not only must the impedance tuning mechanism consider the impedance matching, but also the tuner loss at the different switch states.

For this reason, the fast tuning algorithm presented by Calabrese [13] is used to determine the switch state needed to tune all driven element impedances to the maximum output power and account for tuner losses. The algorithm begins with the switch state of 000000 (all switches off). The power is subsequently measured at the output of each tuner which is fed to each element in the array. The first switch is toggled to the activated state and the output power is measured for improvement. If output power is improved by activation of the first switch, that switch remains activated and the process iterates through the rest of the switches. The algorithm is then re-iterated until no further improvement in output power is accomplished and the switch state that gives the maximum output power is selected [13]. For $\theta_s = 0°$, the search selected the state sequence of 111110. This tuning state was applied to the tuners in all four elements to preserve the linear phase progression of the current sources; maintaining the scan angle and the array pattern shape, and tuning the driven element impedances to the optimum power delivered PA load impedance. As a result of the impedance matching, the achievable resulting transmit power increases from 19.2 dBm to 22.1 dBm, providing 18.2% radar range improvement. The resulting tuned driven element impedances and the resulting array pattern for $\theta_s = 0°$ are shown in Fig. 6, and Fig. 6(b) shows that the array scan angle and overall beam shape remain unharmed, as expected because the same tuning state was used for all four elements.

Fig. 7 shows that tuning inner and outer elements differently can result in undesirable effects on the array pattern. The inner elements were tuned using the switch state sequence of 111110 whereas the outer elements were tuned with the switch state sequence of 000010, which is the state providing the next closest Γ_L to the maximum PA power delivered Γ_L considering tuner losses. Because similar values of Γ_L are presented in all elements, similar impedance matching is achieved. However, many more tuning stubs are exposed in the 111110 state, causing different magnitude and phase adjustments to the currents at the output of the tuners. Removing magnitude and/or phase equality between the different transmitter elements causes the transmitted pattern to be altered, as shown in Fig. 7(b). The antenna gain at the intended scan angle of $\theta_s = 0°$ is reduced from 9.767 dBi to -0.801 dBi (Fig. 7(b)), and the two sidelobes possess higher gain than the desired scan angle. To steer the array to $\theta_s = 0°$, the phases of all current excitations for all elements must be identical. Tuning the outer two elements with a different switch state alters their currents to be out of phase with the inner elements. Fig. 8(a) shows that all four elements have the same transmission phase when the matching networks are tuned to the same switch setting, whereas Fig. 8(b) shows that two different transmission phases exist for the scenario where the outer and inner elements have different matching network switch settings. The 3.55 GHz magnitude and phase of S_{21} are shown in Tables I and II, respectively, for each of the four elements. The difference in S_{21} magnitudes in Fig. 8(a) is small, but the difference in phases between the inner and outer elements is approximately 143°. As such, the phase differences between inner and outer element transmissions seems to be the main cause of the beam distortion visible in Fig. 7(b), when compared to the case where all elements are tuned identically (Fig. 6(b)).

When all elements are not identically tuned, the phase progression can be disrupted, and the array pattern shape will be distorted. The same principle applies across all scan angles.

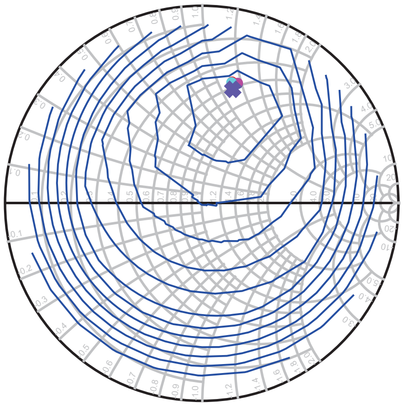

(a)

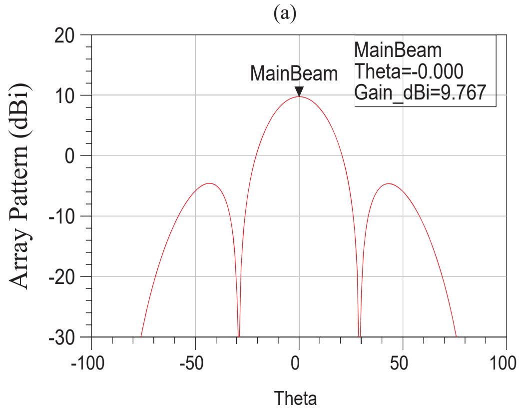

(b)

Fig. 6. (a) Tuned driven element impedances for $\theta_s = 0°$, (b) identically tuned array gain pattern (dBi).

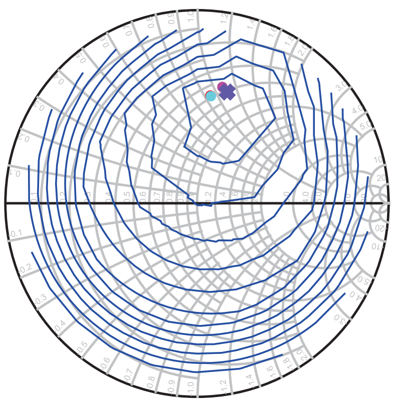

(a)

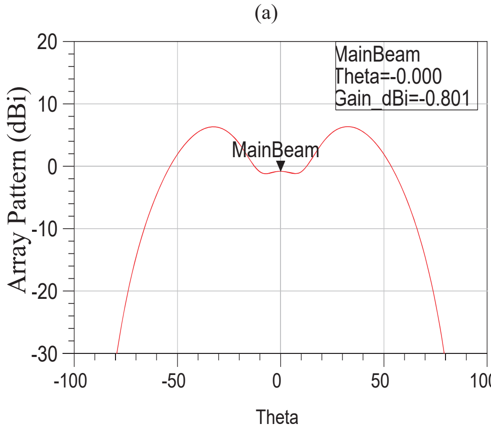

(b)

Fig. 7. (a) Non-identically tuned driven element impedances for $\theta_s = 0°$, (b) Non-identically tuned array gain pattern (dBi).

TABLE I

TUNER TRANSMISSION COEFFICIENTS IDENTICALLY TUNED AT 3.55 GHZ

ELEMENT	$\lvert S_{21} \rvert$	$\angle S_{21}$
1	0.54	38.78°
2	0.54	38.78°
3	0.54	38.78°
4	0.54	38.78°

TABLE II

TUNER TRANSMISSION COEFFICIENTS NON-IDENTICALLY TUNED AT 3.55 GHZ

ELEMENT	$\lvert S_{21} \rvert$	$\angle S_{21}$
1	0.49	-105.08°
2	0.54	38.78°
3	0.54	38.78°
4	0.49	-105.08°

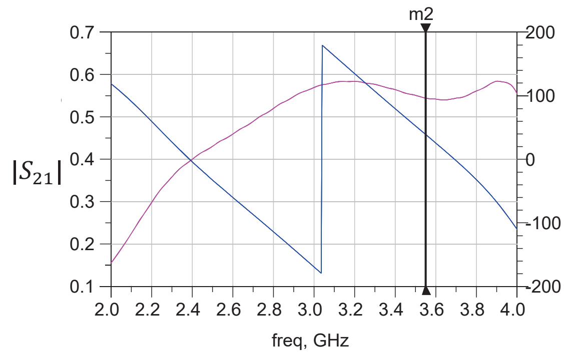

(a)

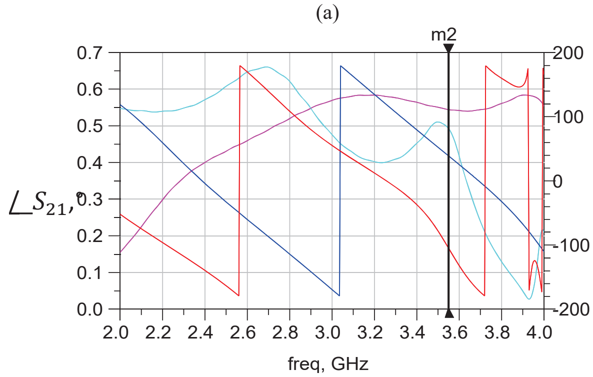

(b)

Fig. 8. (a) Magnitudes (pink, y-axis) and phases (dark blue, right y-axis) of S_{21} of each tuner when tuned with all same switch states, (b) Magnitudes (purple, y-axis) of inner elements, magnitudes (light blue, y-axis) of end elements, phases (dark blue, right y-axis) of inner elements, and phases (red, right y-axis) of S_{21} of each tuner when only inner and outer elements tuned with the same switch states.

B. Tuning at Varying Scan Angles

As the array scan angle θ_s deviates, mutual coupling effects change, and driven element impedances also change, as calculated by equation (6). Figs. 9 and 10 show the initial untuned driven element impedances and array patterns of the four elements when the array is steered to the scan angles of $\theta_s = -60°$ and $+30°$, respectively. The differences between driven impedances of different elements are greater in these scenarios. To maximize output power range for both scan angles, driven element impedances from Fig. 9 must be tuned using the algorithm in [13]. The switched-state stub tuner's load impedance coverage for both of the scan angles (resulting in different driven impedances) at 3.55 GHz is shown in Fig. 11 with the PA maximum-power load impedance.

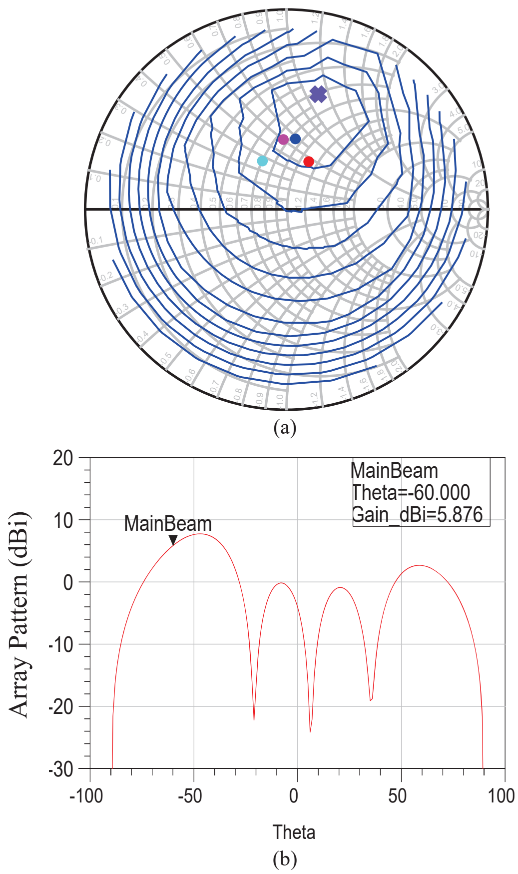

Fig. 9. (a) Untuned driven element impedances for $\theta_s = -60°$, (b) untuned array pattern (dBi).

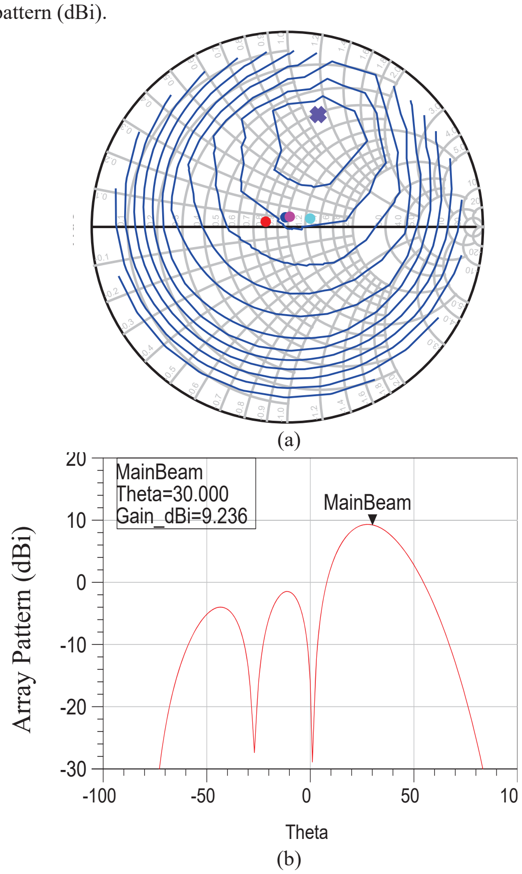

Fig. 10. (a) Untuned driven element impedances for $\theta_s = +30°$, (b) untuned array pattern (dBi).

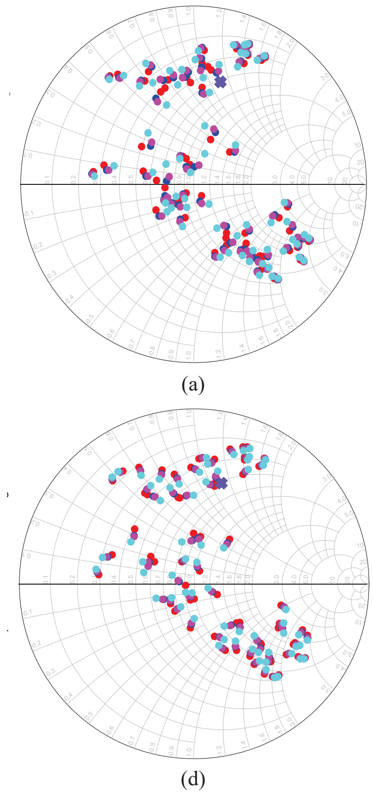

Fig. 11. Tuner element-wise driven impedance coverages (end elements = light blue and red, inner elements = dark blue and purple) for (a) $\theta_s = -60°$, and (b) $\theta_s = +30°$. The maximum-power load impedance is labeled with an 'X'.

TABLE III
ACHIEVABLE TUNED RADAR RANGE IMPROVEMENT

SCAN ANGLE	AVG. INITIAL POWER	AVG. TUNED POWER	RADAR RANGE IMPROVEMENT
-60°	17.2 dBm	21.9 dBm	+26.5%
-25°	18.6 dBm	21.9 dBm	+21.5%
+10°	19.1 dBm	22.1 dBm	+18.9%
+30°	18.3 dBm	22.0 dBm	+23.7%

Implementing the iterative algorithm in [13], the switch state 111110 was once again determined to be the optimal switch state for both scan angles. The same impedance tuner setting was used for all four elements to preserve phase and amplitude consistency in the elements. Calculated range improvements are shown in Table III for four different different scan angles; the calculated radar range improvements vary from 18% to nearly 27%. Figs. 12 and 13 show the beam patterns and element load impedances after tuning has been performed for $\theta_s = -60°$ and $\theta_s = +30°$. The array pattern integrity is preserved, as seen by comparing the tuned patterns (Figs. 12(b), 13(b)) with the untuned patterns (Figs. 10(b)-11(b)), since all elements at each scan angle were tuned using the same switch state. The relative phases of the antenna input currents, therefore, remain the same.

III. CONCLUSIONS

The effects of impedance tuning in the individual elements of a phased array transmitter on detection range capabilities have been demonstrated in a joint circuit and electromagnetic simulation platform. For an EM simulation of four-element,

$\lambda/2$ spaced, microstrip linear, rectangular, and circular arrays, an increase in output power and calculated radar range is achieved through element-wise impedance tuning. Comparison of the tuned array to an un-tuned array results in calculated radar range increases of 18 to 26 percent for broadside and four additional scan angles. While the output power is increased significantly, very little effect on the relative transmission array pattern is observed if the individual elements are tuned identically, because identical tuning preserves the relative magnitude ratios and phase shifts of the element antenna currents. This experiment demonstrates the potential benefits obtainable by placing real-time impedance tuning in the elements of phased array transmitters for radar, with the results extending to fifth-generation (5G) directional wireless communication applications utilizing phased arrays. While size, weight, and power are increased through the addition of the tuner, a tuner properly optimized in real-time greatly benefits the system by allowing increased range and simultaneously preserving the array pattern.

Acknowledgments

The authors wish to thank Keysight Technologies for donation of the Advanced Design System software, and to Modelithics for donation of model libraries to Baylor University through the Modelithics University Program.

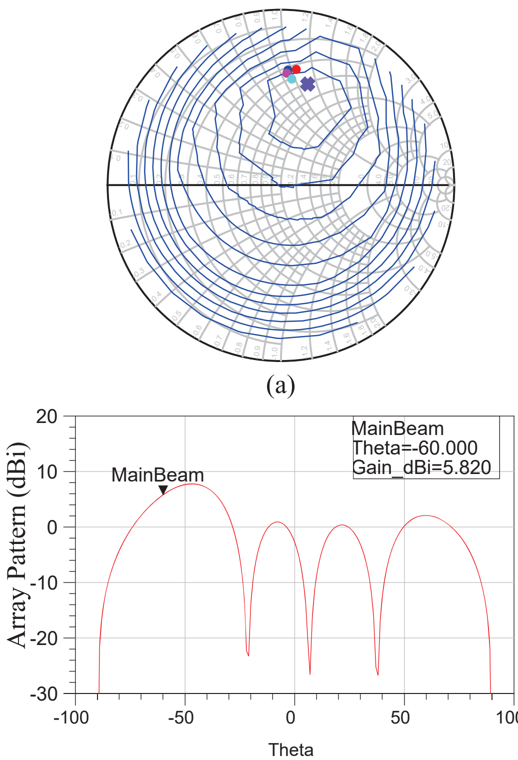

Fig. 12. (a) Tuned driven element impedances at $\theta_s = -60°$, (b) tuned array gain pattern (dBi).

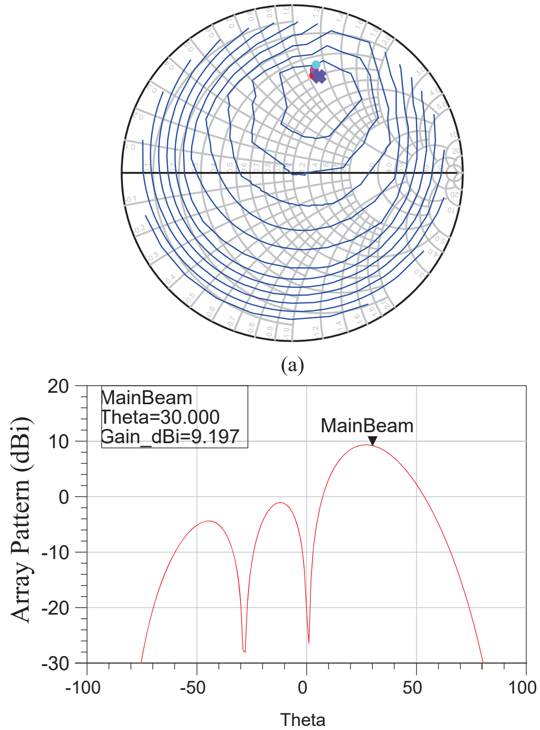

Fig. 13. (a) Tuned driven element impedances at $\theta_s = +30°$, (b) tuned array pattern (dBi).

References

[1] J. Allen, "Gain and Impedance Variation in Scanned Dipole Arrays," *IRE Trans. Antennas and Prop.*, Vol. 10, No. 5, September 1962, pp. 566-572.

[2] D. Qiao *et al.*, "An Intelligently Controlled RF Power Amplifier with a Reconfigurable MEMS-Varactor Tuner," *IEEE Trans. Microwave Theory Tech.*, Vol. 53, No. 3, Mar. 2005, pp. 1089-1095.

[3] C. Baylis *et al.*, "Real-Time Circuit Reconfiguration for a Cognitive Software-Defined Radar Transmission: A New Paradigm in Spectrum Sharing," 2019 IEEE Int'l Symp. Electromagnetic Compatibility, New Orleans, Louisiana, July 2019, pp. 448-450.

[4] A. Semnani *et al.*, "An Electronically Tunable High-Power Impedance Tuner With Integrated Closed-Loop Control," *IEEE Microwave and Wireless Comp. Letters*, Vol. 27, No. 8, Aug. 2017, pp. 754-756.

[5] Y. Sun *et al.*, "Adaptive Impedance Matching and Antenna Tuning for Green Software-Defined and Cognitive Radio," 2011 IEEE 54th Int'l Midwest Symp. Circ. and Sys., Seoul, South Korea, 2011.

[6] Q. Gu *et al.*, "A New Method for Matching Network Adaptive Control," *IEEE Transactions Microwave Theory Tech.*, Vol. 61, No. 1, Jan. 2013, pp. 587-595.

[7] J. de Mingo *et al.*, "An RF Electronically Controlled Impedance Tuning Network Design and its Application to an Antenna Input Impedance Automatic Matching System," *IEEE Trans. Microwave Theory Tech.*, Vol. 52, No. 2, Feb. 2004, pp. 489-497.

[8] J. J. Luther and X. Gong, "A Microstrip Patch Phased Array Antenna with Parasitic Elements and Reactance-Tuned Coupling," 2011 IEEE Int'l Symp. Antennas and Prop., Spokane, Washington, 2011, pp. 3291-3294.

[9] E. Magill and H. Wheeler, "Wide-Angle Impedance Matching of a Planar Array Antenna by a Dielectric Sheet," *IEEE Trans. Antennas Prop.*, Vol. 14, No. 1, Jan. 1966, pp. 49-53.

[10] R. Xia *et al.*, "Experimental Investigation of Wide-Angle Impedance Matching of Phased Array Using Overlapped Feeding Network," *IEEE Antennas and Wireless Prop. Letters*, Vol. 13, 2014, pp. 1284-1287.

[11] T. V. Sikina, "Wide Angle Impedance Matching Techniques for Volumetrically Scanned Phased Arrays," 2010 IEEE Int'l Symp. Phased Array Sys. and Tech., Waltham, Massachusetts, 2010, pp. 924-929.

[12] R.L. Haupt, *Antenna Arrays: A Computational Approach*, Wiley-IEEE Press, 2010.

[13] C. Calabrese *et al.*, "Fast Switched-Stub Impedance Tuner Reconfiguration for Frequency and Beam Agile Radar and Electronic Warfare Applications," 2020 IEEE Int'l Radar Conf., Washington, D.C., April 2020.